Article ID: 1007-8827(2010)02-081-08

Self-sustaining high-temperature synthesis of carbon-encapsulated magnetic nanoparticles from organic and inorganic metal precursors

M. Bystrzejewski[1,2], M. Szala[3], W. Kiciński[3], W. Kaszuwara[4], M. H. Rummeli[2], T. Gemming[2], A. Huczko[1]

(1. *Dept of Chemistry, Warsaw University, Pasteur* 1 *str.*, 02-093 *Warsaw, Poland*;
2. *IFW Dresden, Helmholtzstr.* 20, 01069 *Dresden, Germany*;
3. *Military University of Technology, Kaliskiego* 2, 00-908 *Warsaw, Poland*;
4. *Warsaw University of Technology, Woloska* 141, 02-507 *Warsaw, Poland*)

Abstract: A systematic study on the synthesis of carbon-encapsulated magnetic nanoparticles by self-sustaining high-temperature synthesis (SHS) is presented. The SHS was carried out using NaN_3 as a reducer; and poly(tetrafluoroethene) $(C_2F_4)_n$, hexachloroethane (C_2Cl_6) and hexachlorobenzene (C_6Cl_6) as three various oxidizers. The effect of metal precursor, ($Fe(CO)_5$ or $K_3[Fe(CN)_6]$) on the yield, reaction heat, morphology, structure and magnetic properties of the products was investigated. The highest product yield with best magnetic characteristics was obtained from the organometallic iron precursor and C_2Cl_6 oxidizer.

Keywords: Self-propagating high-temperature synthesis (SHS); Combustion synthesis; Magnetic nanoparticles, Carbon nanostructures

CLC number: TB 383 **Document code**: A

1 Introduction

Self-sustaining high-temperature synthesis (SHS) is a well-known method for preparation of many useful compounds, such as high temperature carbides, nitrides, oxides and hydrides[1]. The SHS route is based on chemical reactions occurring within a narrow high-temperature (1 000-3 000 K) zone, which propagates in a starting mixture of oxidizer and reducer powders. Propagation of the high-temperature zone is also called a combustion wave. SHS is a fast, one-step efficient process that uses simple and low-cost starting materials. It was found recently that SHS reactions can lead to formation of interesting nanomaterials, such as nanoparticles[2], carbon-encapsulated magnetic nanoparticles (CEMNPs)[3], exfoliated graphite[4], nanowires and nanotubes[4-6].

Metallic nanoparticles attract an increasing interest, owing to their size-dependent magnetic response[7]. It is also reflected in their wide prospective applications, e. g. in data storage[8], catalysis and numerous biomedical issues (drug delivery system, contrast agents in magnetic resonance imaging)[9]. The largest disadvantage of magnetic nanoparticles is their low stability against oxidation and agglomeration, which limits their use under ambient conditions. Various encapsulating routes have been proposed to enhance the nanoparticles´stability. Most of the common coating materials (e. g. organic molecules, surfactants and polymers) isolate the nanoparticles very well; however, they have a low thermal and mechanical stability. Encapsulating by carbon is free from these drawbacks. Carbon coatings are light, have a high thermal stability and allow for further CEMNP modifications via wet chemistry routes.

CEMNPs are formed through a rapid quenching of high-temperature-gas containing carbon species and a vapour of the metal to be encapsulated. The highest yields in CEMNP synthesis have been so far observed for various plasma routes[10]. SHS synthesis, in contrary to technologically advanced plasma techniques, is a relatively simple method that can be used for synthesis of CEMNPs. So far, CEMNPs have been synthesized via SHS route, where reactant mixtures containing NaN_3 and C_6Cl_6 were used for the reducer and oxidizer, respectively. CEMNP yield strongly depen-

Received date: 2009-11-09; **Revised date**: 2010-03-24

Author introduction: Michal Bystrzejewski (1980 –), male, Ph. D., Assistant Professor, engaged in the reserach of carbon nanomaterials.
E-mail: mibys@chem.uw.edu.pl, Fax: + 48 22 822 59 96

English edition available online ScienceDirect (http://www.sciencedirect.com/science/journal/18725805).
DOI: 10.1016/S1872-5805(09)60017-2

ded on the metallic precursor, i. e. in the case of ferrocene[11] the yield was 10 times as high as that from ultrafine metal powders[12]. The present study is focused on various SHS reactant systems, which differ in the heats of reaction. Such an approach is suitable, since it causes high temperatures during the course of the reactions and increases the process efficiency. Moreover, the influence of two various metallic precursors (organic and inorganic) on the yield, morphology, structure and magnetic properties are studied.

2 Experimental

Compositions of the mixtures (Table 1) investigated were calculated on the basis of assumed stoichiometric equations leading to the formation of sodium chloride (or fluoride), free carbon and gaseous nitrogen. The maximum content of the Fe precursor in the mixtures was experimentally selected. Higher Fe/C ratios yielded no reaction at all. Starting mixtures were prepared in a ceramic mortar by dry mixing powders of oxidizer, reducer and Fe precursor. In all tested systems, sodium azide was used as a reducer, whilst $(C_2F_4)_n$, C_2Cl_6 and C_6Cl_6 were used as efficient oxidizers. All compounds, having purity higher than 99.9%, were used. The grain size of all solid reagents was 5-20 μm. Two compounds, iron pentacarbonyl $Fe(CO)_5$ and potassium ferricyanide (III) $K_3[Fe(CN)_6]$, were selected as organic and inorganic Fe precursors, respectively.

Table 1　Operational parameters

Test	Initial mixture	Composition *w*/ %	Fe/C (Atom percent)	Reaction heat *e*/kJ•kg^{-1}	Solid product yield *w*/ %	Yield after purification *w*/ %
1	$(C_2F_4)_n/NaN_3/Fe(CO)_5$	25.0/65.6/9.50	6.5	3696	15.8	16.7
2	$C_2Cl_6/NaN_3/Fe(CO)_5$	31.7/51.7/16.6	12.2	2 917	60.8	25.0
3	$C_6Cl_6/NaN_3/Fe(CO)_5$	35.0/48.3/16.7	7.3	3090	60.2	29.4
4	$(C_2F_4)_n/NaN_3/K_3[Fe(CN)_6]$	57.3/22.9/45.8	12.1	2078	70.1	25.0
5	$C_2Cl_6/NaN_3/K_3[Fe(CN)_6]$	27.1/47.9/25.0	14.3	2798	75.4	60.0
6	$C_6Cl_6/NaN_3/K_3[Fe(CN)_6]$	31.1/43.0/25.9	7.0	2793	50.0	35.0
1 *	$(C_2F_4)_n/NaN_3$	72.2/27.8		3 460	33.0	
2 *	C_2Cl_6/NaN_3	37.8/62.2		2388	60.0	
3 *	C_6Cl_6/NaN_3	42.2/57.8		3005	64.0	

Note: Solid product yield is referred to as the mass of initial target

Approximately 5 g of pulverized and mixed samples were placed in a graphite crucible and put into a calorimetric bomb (275 cm^3 in volume), which was sealed and filled by argon to an initial pressure of 1.0 MPa. The SHS process was initiated with an electrically heated resistance wire (Kanthal). The calorimetric bomb was inserted in a water calorimeter to measure the reaction heat. The solid combustion products were removed from the bomb with water. The suspension was filtered and the deposit obtained was washed with ethanol. After drying, the reaction products were weighed and analysed to identify their morphology. Next, the products were subjected to a purification procedure (24 h boiling in 30% HCl, washing with the excess of water and ethanol) to remove the as-formed inorganic salts (e. g. NaCl, Prussian blue) and non-encapsulated iron nanoparticles.

The products morphology was studied by scanning and transmission electron microscopy. Phase composition was investigated by powder X-ray diffraction (Cu K-alpha radiation, 0.01° step size). Raman spectroscopy (514.5 nm excitation laser, 2 cm^{-1} spectral resolution) was applied to study structural details of carbon phase. Magnetic characteristics were measured by a vibrating magnetometer at room temperature.

3 Results and discussion

Compositions of the mixtures are presented in Table 1. The reaction heat was obtained by averaging three experimental values. The amounts of the raw combustion products recovered from the reactor were referred to the initial mass of the sample. The heats and raw product yield were also measured for the reactions without iron precursor (marked with an asterisk) as a comparison.

All the reactions are fast and exothermic, which are enough to proceed in a self-sustaining regime. The reaction heat differs in a relatively narrow window between 2078 and 3696 kJ/kg. The small difference in the measured heat suggests that the temperature in the combustion wave be similar for all the mixtures investigated. The addition of iron pentacarbonyl leads to an increase in the reaction heat in all systems. The presence of potassium ferricyanide (III) general-

ly decreases the reaction heat; however, the C_2Cl_6/NaN_3 mixture is an exception. The physical states that are different for the two iron precursors presumably influence the heat effects. At ambient conditions, iron pentacarbonyl is a volatile liquid (m. p. 253 K, b. p. 286 K) and can react directly in vapour phase with the combustion products from halogenocarbons and sodium azide. In contrast to iron pentacarbonyl, $K_3[Fe(CN)_6]$ is a crystalline solid which melts and decomposes at about 600 K. The melting and decomposition processes of potassium ferricyanide are highly endothermic. Thus, some amounts of heat generated in the combustion wave are absorbed through the melting and decomposition of $K_3[Fe(CN)_6]$. An increased heat in Test 5 suggests that the as-generated species from the precursor may interact with the combustion wave via other route.

The solid product yield changes little for the C_2Cl_6/NaN_3 reaction system (Tests 2, 5 and 2*) and C_6Cl_6/NaN_3 reaction system (Tests 3, 6 and 3*) as shown in Table 1. The iron precursors (organic and inorganic) have no significant influence in the yield of solid products for the two systems. However, larger variations were found for C_2F_4/NaN_3 reaction system (Tests 1, 4 and 1*). The yield in Test 4, which is ca. 2 times as high as that in the reference Test 1*, resulted from the presence of the un-decomposed Fe precursor (it will be discussed later). The yield in Test 1 achieved a half of the efficiency for Test 1*. This could be accounted for by the fact that the reaction heat in Test 1 is higher than that in Test 1*, which might cause a gasification of relevant solid product (e. g. carbon) and, therefore, decreases the yield.

The values of purification yield show how much of the sample remained after acid treatment. The mass loss (40-87%) was caused by the presence of by-products and the fraction of iron that was not encapsulated by carbon. The largest mass reduction was observed for Test 5, in which the content of Fe (in respect to C) was the highest. This could be caused by the un-encapsulated Fe that dissolved in 30% HCl. Therefore, the purification yields can be used for a rough estimation of encapsulating efficiency.

SEM images of combustion products after purification are shown in Fig. 1. Spheroid carbon particles were seen in each sample, which had a diameter ranging from 50 to 200 nm. Some particles had slightly elongated shapes and aggregated into large sphere-like assemblies (Fig. 1b, d). Importantly, none of the sample contained the non-encapsulated iron particles, indicating that the purification was successful. All synthesis routes for CEMNPs yield some amounts of the assembled particles in micrometer size[11-12].

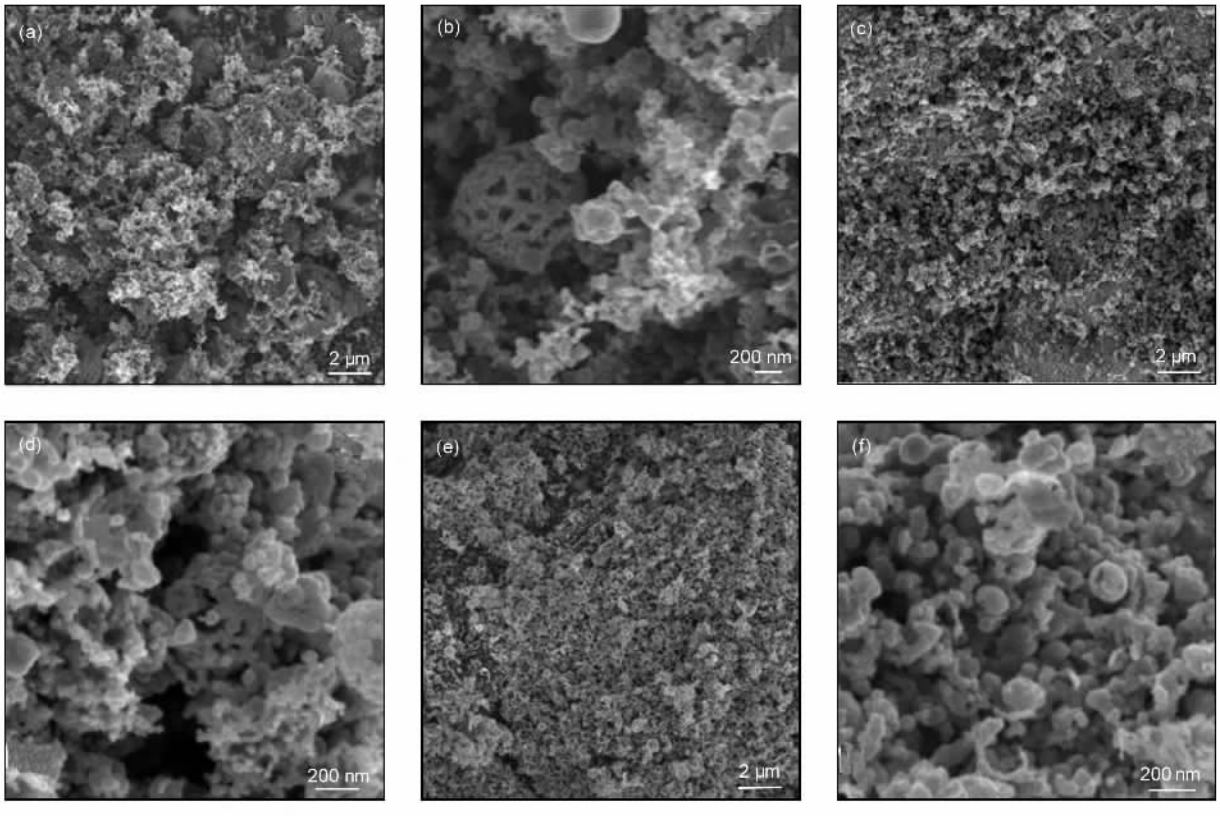

Fig. 1　SEM images of purified the products: a, b test 1, c, d test 2, e, f test 5

Further morphological details of the purified products were obtained from TEM microscopy (Fig. 2). All investigated samples had the similar morphology. Three types of nanostructures were found in samples, which were CEMNPs, hollow carbon capsules and amorphous carbon. CEMNPs had a diameter between 20 and 100 nm and had perfect spherical shapes. The magnetic cores were tightly covered by carbon with a thickness of a few nanometer (Fig. 2c). Hollow capsules indicated in Fig. 2b were in a diameter range between 20 and 50 nm, which had empty cores and more defected structure compared with CEMNPs. It was apparent that they had been filled with metallic particles, but the purification procedure leached off the encapsulated materials. The observed morphology did not show any substantial differences compared with the products obtained from the NaN_3/C_6Cl_6/Ferrocene mixture[11]. This demonstrated that SHS route was quite selective and depends little on metallic precursor used.

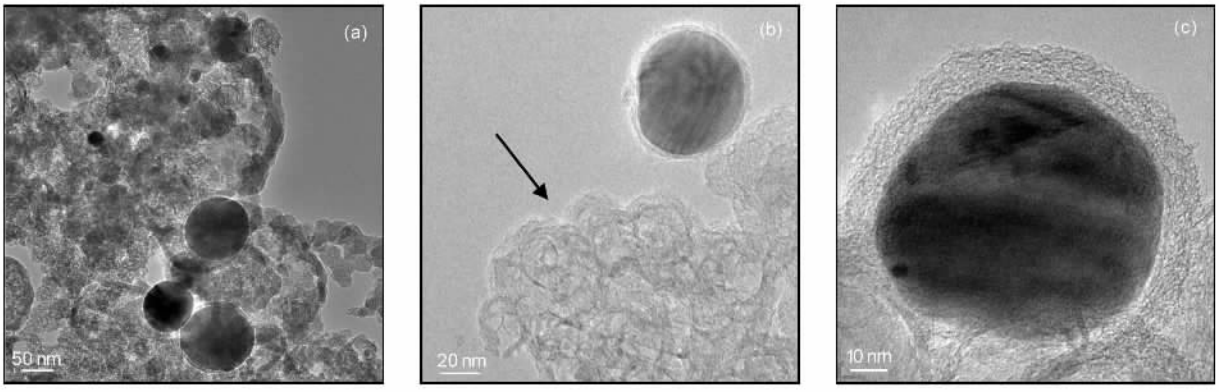

Fig. 2　TEM images of the purified product from Test 1

Powder X-ray diffraction was used to evaluate the phase composition of the products. Selected patterns are shown in Fig. 3, whilst the detailed compositions are listed in Table 2. The products obtained from metal organic precursor (Tests 1-3) were composed of carbon, Fe, NaCl and Prussian blue ($Fe_4[Fe(CN)_6]_3$). In each case, a solid solution of carbon in *bcc* Fe was detected (termed as Fe-C). The lack of peaks ascribed to the starting reagents showed that all the SHS reactions had proceeded completely. The presence of Prussian blue suggested that nitrogen and carbon evolved during the course of reaction react with iron, leading to the formation of this complex salt. All diffraction peaks except for carbon were relatively narrow, which showed that both iron and inorganic particles had a high crystalline order. The (002) carbon peak was substantially broadened, suggesting that the graphitization degree was low. Shape analysis of the (002) diffraction peak is usually performed to derive basic structural data, e. g. average interlayer distance, mean crystallite size. However, the (002) carbon reflexes overlapped with other diffraction signals, making any quantitative structural analysis of the carbon phase inaccurate. Products obtained using inorganic metal precursors (Tests 4-6) had similar phase compositions. In addition, KCl was detected in these samples. This demonstrated that K resulted from the decomposition of iron precursor reacted with chlorine. Interestingly, the product from Test 4 contained also the initial iron precursor, indicating a incomplete decomposition of $K_3[Fe(CN)_6]$. In fact, the reaction heat for Test 4 was the lowest, which might be the cause of insufficient decomposition of the iron precursor. Purification resulted in a nearly complete elimination of inorganic by-products (NaCl, NaF, KCl, $Fe_4[Fe(CN)_6]_3$) and non-encapsulated iron nanoparticles. Selected diffraction pattern for the purified sample is shown in Fig. 3c. Weak signals appearing at ca. 31° and 51° may be ascribed to (200) and (440) lattice planes of NaCl and Prussian blue, respectively, in each purified sample (Tests 1-6). This suggested that some amounts of these inorganic materials were also retained after acid treatment. These materials could be rather embedded in amorphous carbon nanoparticles, which were difficult to be leached off. Importantly, *fcc* Fe was found in none of the samples (raw and purified). *Fcc* Fe is a metastable form of iron at room temperature; however, it frequently occurs in CEMNPs[13]. Encapsulation of *fcc* Fe is highly undesired, because of its very low-magnetic susceptibility.

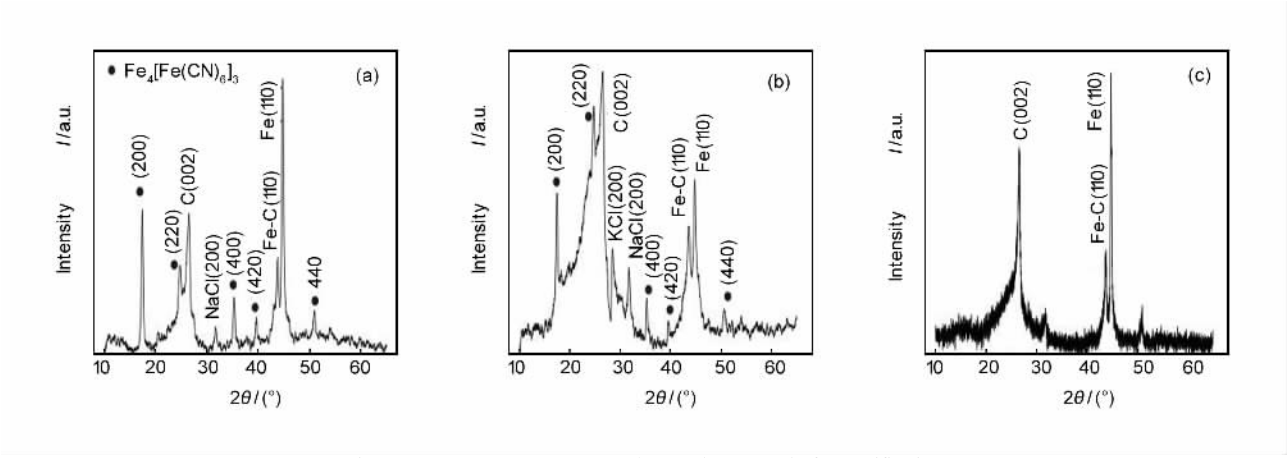

Fig. 3　XRD patterns: a-Test 2, b-Test 5, c-Test 5 after purification

Table 2　Phase compositions, structural and magnetic characteristics of products

Test	Initial compositions	Phase compositions	G/D	G band FWHM σ/cm^{-1}	H_c/Gs	M_s/emu•g^{-1}
1	$(C_2F_4)_n/NaN_3/Fe(CO)_5$	C, *bcc* Fe, Fe-C, NaF, $Fe_4[Fe(CN)_6]_3$	1.02	71	242	9.4
2	$C_2Cl_6/NaN_3/Fe(CO)_5$	C, *bcc* Fe, Fe-C, NaCl, $Fe_4[Fe(CN)_6]_3$	0.75	87	213	14.4
3	$C_6Cl_6/NaN_3/Fe(CO)_5$	C, *bcc* Fe, Fe-C, NaCl, $Fe_4[Fe(CN)_6]_3$	0.70	89	230	9.9
4	$(C_2F_4)_n/NaN_3/K_3[Fe(CN)_6]$	C, *bcc* Fe, NaF, KCl, $K_3[Fe(CN)_6]_3$	0.28	128	248	2.3
5	$C_2Cl_6/NaN_3/K_3[Fe(CN)_6]$	C, *bcc* Fe, Fe-C, NaCl, KCl, $Fe_4[Fe(CN)_6]_3$	0.42	95	166	2.0
6	$C_6Cl_6/NaN_3/K_3[Fe(CN)_6]$	C, *bcc* Fe, Fe-C, NaCl, KCl, $Fe_4[Fe(CN)_6]_3$	0.49	93	297	1.2

The structural features of carbon phases were obtained from Raman spectra (Fig. 4a). The spectra were collected within the range of 600-2 000 cm^{-1}, which is the most valuable region providing the structural details of carbon materials. There are two bands appearing at 1 350 and 1 590 cm^{-1}. The latter feature, the so-called G band, is related to stretching C—C vibrations in graphene layers[14]. The D band corresponds to disorder and this feature becomes active by the presence of structural and topological defects (e. g. sp^3 carbons, vacancies, dangling bonds, foreign atoms substituted in graphitic layers). The G/D integral intensity ratio is a well-accepted indicator of average sample crystallinity[14]. The width of the G band is related to the extent of disorder within the graphitic planes. Recent literature reports that the FWHM of the G band is also capable for diagnostics because it can be used for rough estimation of the ordering between the parallel stacked graphitic layers in carbon particles[15]. A brief evaluation of the spectra indicated that the samples differed in crystallization. The values of G/D ratios and FWHMs of the G band are listed in Table 2. They were obtained from deconvolution of spectra using Lorentzian functions. The products obtained in Tests 1-3 were better graphitized, and this was reflected by the larger G/D ratios and narrower widths of the G band. Generally, the graphitization degree strongly depends on the reaction temperature. For example, samples are often exposed to high temperatures (2 500-3 500 K) to improve the graphitization of carbon materials[16]. In our case, the temperatures obtained in the SHS reactions should be very different, because the reaction heat varied within a broad window (Table 1). Thus, the Raman parameters should correspond to the heat, which is plotted in Fig. 4b. In fact, both the G/D ratios and the FWHMs changed monotonically with the enthalpy of reaction (Fig. 4b).

All products had weak ferromagnetic properties (Fig. 5, Table 2). The coercive forces (H_c) were relatively small and between 166 and 297 Gs. The differences in H_c values were likely due to distinct size distribution of CEMNPs in the samples[17]. The remnant magnetizations did not exceed 7-9% of the saturation magnetization (M_s). The saturation limit was achieved for all samples below a field of 10 kGs (1 T). This is of great importance for applications, because the maximum magnetic response of carbon encapsulates is accomplished at relatively low-magnetic fields, which are available from common permanent magnets. The samples had various values of the saturation magnetization. The M_s values can be used for semi-quantitative analysis of Fe content in the samples. It is possible to do this by making a reasonable assumption that only iron nanoparticles contribute to the overall magnetic moment as the magnetic susceptibilities of carbon, NaCl or Prussian blue are a few orders of magnitude lower as compared with Fe. The

saturation magnetization for pure *bcc* Fe is 224 emu/g[18]. Products obtained from $Fe(CO)_5$ have ca. 5-7 times as high as Fe contents for samples synthesized from inorganic metal precursors. These differences could be caused by the following factors: (i) reaction heat, (ii) thermal stability of Fe precursor, (iii) initial Fe content. $Fe(CO)_5$ under ambient conditions is a liquid, whilst $K_3[Fe(CN)_6]$ forms crystallites. The two precursors have very distinct energy to break iron-carbon bonds and to form iron clusters, which is 122 kcal[19] and 422 kcal[20] for $Fe(CO)_5$ and $K_3[Fe(CN)_6]$, respectively. This is why the products synthesized from inorganic Fe precursor had a lower content of CEMNPs. The low-reaction heat in Tests 4-6 also observed this rule.

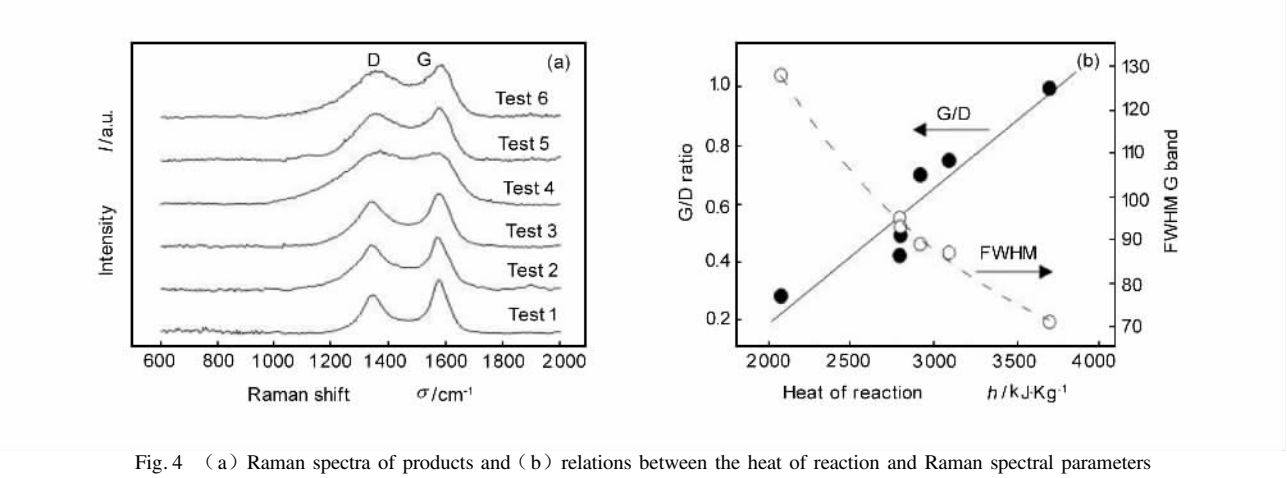

Fig. 4 (a) Raman spectra of products and (b) relations between the heat of reaction and Raman spectral parameters (full circles refer to G/D, open circles to FWHM)

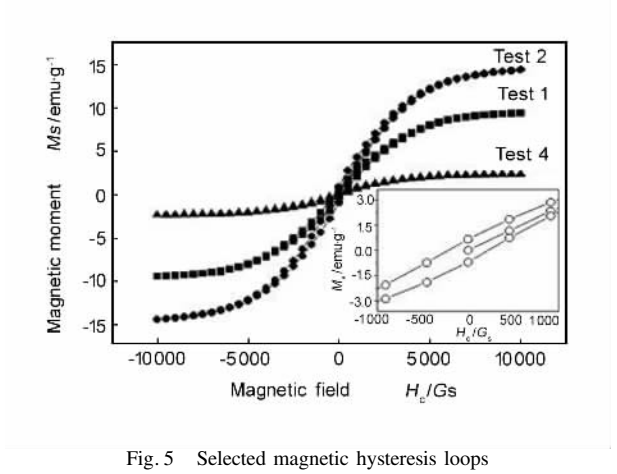

Fig. 5 Selected magnetic hysteresis loops

The measurements of magnetic parameters were done on purified samples only. The magnetic characteristic for the as-obtained products should be different. This is because the non-encapsulated Fe particle also contributed to the magnetic response and primarily increased the magnetic moments. The effect of purification on magnetic response of CEMNPs obtained by three different synthesis routes (arc plasma, plasma jet and SHS) had been studied in a recent paper[21]. It had been shown that the M_s was decreased by a factor of even 5 after purification.

The values of saturation magnetization, as shown above, demonstrated how much of encapsulated iron nanoparticles were present in purified products. Direct comparison of the M_s for CEMNPs obtained in different route can indicate which route is the most favourable for CEMNP fabrication. The SHS synthesis of carbon-encapsulated iron nanoparticles was also accomplished using fine Fe powders as metal precursors[12]. In that case, M_s values were between 1.0 and 1.3 emu/g. This showed that the use of molecular precursors of iron increased the yield of the reaction by many-fold (e.g. Test 1). Carbon arc technique is more efficient fabrication technique, because the purified products obtained in this route have the M_s of 60-70 emu/g[21]. The reactors using flowing plasma jets are the most productive systems, because they are operated under continuous conditions and produce the products with saturation magnetization exceeding 96 emu/g[22]. Aside from the M_s, the coercive force is a parameter that determines the magnetic response. The obtained H_c values (166-297 Gs) are generally close to the coercive fields for CEMNPs fabricated by SHS (60-224 Gs)[11-12], carbon arc (247 Gs)[13], plasma jet (133-242 Gs)[22]. The demonstrated variations are small, which result from the different size distributions of CEMNPs.

4 Conclusions

Self-sustaining synthesis of CEMNPs was systematically studied. The synthesis was based on high temperature combustion zone propagation through the reactor with the simultaneous production of carbon species and decomposition of iron precursor. The

driving force resulting in the high temperature environment was a rapid reaction between a reducer and three various oxidizers, leading to a rapid heat production. The influence of two distinct metal precursors, $Fe(CO)_5$ and $K_3[Fe(CN)_6]$, on process yield, morphology, structure and magnetic properties was studied. The use of potassium ferricyanide drastically decreased the reaction heat and the CEMNPs yield. The iron precursors did not influence the average size and phase composition of CEMNPs. All products had weak ferromagnetic behaviour with coercive forces between 166 and 297 Gs. The highest CEMNPs yield was achieved in $NaN_3/C_2Cl_6/Fe(CO)_5$ mixture.

References

[1] Varma A, Rogachev A, Mukasyan A, et al. Combustion synthesis of advanced materials: principles and applications[J]. Advanced Chemical Engineering, 1998, 24: 78-226.

[2] de Basi R, Figueiredo A, Fernandes A, et al. Synthesis of cobalt ferrite nanoparticles using combustion waves[J]. Solid State Communications, 2007, 144: 15-17.

[3] Bystrzejewski M, Huczko A, Lange H, et al. Carbon-encapsulated magnetic nanoparticles spontaneously formed by thermolysis route[J]. Fullerenes, Nanotubes and Carbon Nanostructures, 2008, 16: 217-230.

[4] Szala M. Combustion synthesis of hollow carbon fibers[J]. International Journal of Self-Propagating High-Temperature Synthesis, 2008, 17: 106-111.

[5] Huczko A, Bystrzejewski M, Lange H, et al. Combustion synthesis as a novel method for production od 1-D SiC nanostructures[J]. Journal of Physical Chemistry B, 2005, 109: 16244-16251.

[6] Huczko A, Osica M, Rutkowska A, et al. A self-assembly SHS approach to form silicon carbide nanofibers[J]. Journal of Physics: Condensed Matter, 2007, 19: 395022.

[7] Prandolini M, Magnetic nanostructures: radioactive probes and recent developments[J]. Reports on Progress in Physics, 2006, 69: 1235-1324.

[8] Reiss G, Hutten A. Magnetic nanoparticles: applications beyond data storage[J]. Nature Materials, 2005, 4: 725-726.

[9] Pankhurst Q A, Connolly J, Jones S K, et al. Applications of magnetic nanoparticles in biomedicine[J]. Journal of Physics D: Applied Physics, 2003, 36: R167-181.

[10] Fujimaki S, Yatsue T, Kokaku Y, et al. Preperation of ultra-thin carbon overcoat for magnetic recording medium by filtered cathodic vacuum arc technology[J]. Vacuum, 2004, 74: 711-716.

[11] Bystrzejewski M, Huczko A, Lange H, et al. Combustion synthesis route to carbon-encapsulated iron nanoparticles[J]. Diamond and Related Materials, 2007, 16: 225-228.

[12] Bystrzejewski M, Huczko A, Soszyński M, et al. An easy one-step route to carbon-encapsulated magnetic nanoparticles[J]. Fullerenes, Nanotubes and Carbon Nanostructures, 2009, 17: 1-16.

[13] Borysiuk J, Grabias A, Szczytko J, et al. Structure and magnetic properties of carbon encapsulated Fe nanoparticles obtained by arc plasma and combustion synthesis[J]. Carbon, 2008, 46: 1693-1701.

[14] Barros E, Demir N, Souza Filho A, et al. Raman spectroscopy of graphitic foams[J]. Physical Review B, 2005, 71: 165422.

[15] Yoshida A, Kaburagi Y, Hishiyama Y. Full width at half maximum intensity of the G band in the first order Raman spectrum of carbon materials as a parameter for graphitization[J]. Carbon, 2006, 44: 2333-2335.

[16] BłaŽewicz S, Świątkowski A, Trznadel B. The influence of heat treatment on activated carbon structure and porosity[J]. Carbon, 1999, 37: 693-700.

[17] Sun Y, Gao R, Feng W, et al. Effect of grain size and distribution on the anisotropy and coercivity of nanocrystalline $Nd_2Fe_{14}B$ magnets[J]. Journal of Magnetism and Magnetic Materials, 2006, 306: 108-111.

[18] Zhao X, Liu B, Liang Y, et al. Structure and magnetic properties of the oxide layers on iron ultrafine particles[J]. Applied Physics A, 1997, 64: 483-486.

[19] Barnes L, Rosi M, Bauschlicher C. An *ab initio* study of $Fe(CO)_n$ $n=1,5$ and $Cr(CO)_6$[J]. Journal of Chemical Physics, 1991, 94: 2031-2039.

[20] Redondo P, Rayan V, Valdes H, et al. A theoretical study of the $[FeCN]^+$ system: Cyanide isocyanide competition and isomerization barrier[J]. Chemical Physics Letters, 2007, 445: 22-27.

[21] Bystrzejewski M, Grabias A, Borysiuk J, et al. Mössbauer spectroscopy of carbon-encapsulated magnetic nanoparticles obtained by different routes[J]. Journal of Applied Physics, 2008, 104: 54307.

[22] Bystrzejewski M, Karoly Z, Szepvolgyi J, et al. Continuous synthesis of carbon encapsulated magnetic nanoparticles with a minimum production of amorphous carbon[J]. Carbon, 2009, 47: 2040-2048.

由有机和无机金属前躯体自蔓延高温合成碳包覆磁纳米粒子

M. Bystrzejewski[1,2], M. Szala[3], W. Kiciński[3], W. Kaszuwara[4], M. H. Rummeli[2], T. Gemming[2], A. Huczko[1]

(1. Dept of Chemistry, Warsaw University, Pasteur 1 str., 02-093 Warsaw, Poland;
2. IFW Dresden, Helmholtzstr. 20, 01069 Dresden, Germany;
3. Military University of Technology, Kaliskiego 2, 00-908 Warsaw, Poland;
4. Warsaw University of Technology, Woloska 141, 02-507 Warsaw, Poland)

摘 要: 介绍了一项由自蔓延高温合成(SHS)碳包覆磁纳米粒子的系统研究。采用还原剂 NaN_3 和三种不同氧化剂 – 聚四氟乙烯、六氯乙烷和六氯苯,实施了 SHS 制备。研究了金属前躯体($Fe(CO)_5$ 或 $K_3[Fe(CN)_6]$)对产物的得率、反应热、形貌、结构和磁性能的影响。结果表明:有机铁前躯体和 C_2Cl_6 氧化剂反应体系可获得磁性最佳、得率最高的产物。

关键词: 自蔓延高温合成(SHS);燃烧合成;磁纳米粒子;碳纳米结构

作者简介: Michal Bystrzejewski (1980 –), 男,博士,副教授,主要从事炭纳米材料的研究.
E-mail: mibys@chem.uw.edu.pl, Fax: + 48 22 822 59 96

炭专业文献中的关键词(Keywords for carbons)
—炭的类型(Tpyes of carbon)

Activated carbon 活性炭
Battery carbon 电池用炭
Carbon aerogel 炭气凝胶
Carbon beads 炭珠
Carbon black 炭黑
Carbon cloth 炭布
Carbon clusters 碳簇
Carbon composites 炭复合物
Carbon fibers 炭纤维
Carbon filaments 炭丝
Carbon films 炭膜
Carbon ocoils 螺旋形炭
Carbon nanotubes 纳米碳管
Carbon nanostructure 碳纳米结构
Carbon onions 洋葱状碳
Carbon precursor 炭前驱体
Carbon xerogels 炭干凝胶
Carbon/carbon composites 炭/炭复合材料
Carbyne 碳炔
Catalytically grown carbon 催化生长炭
Char 半焦
Charcoal 木炭
Chemically modified carbons 化学改性炭
Coal 煤
Coal tar pitch 煤焦油沥青
Coke 焦炭
Diamond 金刚石
Diamond-like carbon 类金刚石
Doped carbons 掺杂炭
Electrodes 电极
Exfoliated graphite 膨胀石墨
Fullerene 富勒烯
Glass-like carbon 玻璃炭
Graphite 石墨
Graphite oxide 石墨氧化物
Graphitic carbon 石墨化炭
Highly oriented graphite 高定向石墨
Intercalation compounds 层间化合物
Isotropic carbon 各向同性炭
Isotropic graphite 各向同性石墨
Kish graphite Kish 石墨
Mesophase 中间相
Mesophase pitch 中间相沥青
Molecular sieves 分子筛
Natural graphite 天然石墨
Needle coke 针状焦
Non-graphitic carbon 非石墨化炭
Nuclear graphite 核石墨
Petroleum coke 石油焦
Petroleum pitch 石油沥青
Pitch 沥青
Porous carbon 多孔炭
Pyrolytic carbon 热解炭
Resins 树脂
Single crystals 单晶
Soot 烟炱
Synthetic graphite 人造石墨
Tars 焦油
Vapor grown carbon 气相生长炭
Whiskers 晶须

(李峰,王茂章 供稿)